Easy Synthesis and Magnetic Properties of Iron Oxide Nanoparticles

ARTICLE *in* CHEMISTRY OF MATERIALS · JUNE 2004

Impact Factor: 8.35 · DOI: 10.1021/cm049552x

7 AUTHORS, INCLUDING:

Kyoungja Woo
Korea Institute of Science and Technology
51 PUBLICATIONS **1,069** CITATIONS
SEE PROFILE

Chul Sung Kim
Kookmin University
200 PUBLICATIONS **932** CITATIONS
SEE PROFILE

Easy Synthesis and Magnetic Properties of Iron Oxide Nanoparticles

Kyoungja Woo,*,† Jangwon Hong,† Sungmoon Choi,† Hae-Weon Lee,† Jae-Pyoung Ahn,† Chul Sung Kim,‡ and Sang Won Lee‡

Nano-Materials Research Center, Korea Institute of Science and Technology, P.O. Box 131, Cheongryang, Seoul 130-650, Korea, and Department of Physics, Kookmin University, Seoul 136-702, Korea

Received March 17, 2004. Revised Manuscript Received May 10, 2004

Easy preparation of iron oxide nanoparticles [5- and 11-nm maghemite (γ-Fe_2O_3) and 19-nm magnetite (Fe_3O_4)] by thermal decomposition of $Fe(CO)_5$ in the presence of residual oxygen of the system and by consecutive aeration were investigated by TEM/HRTEM, XRD, and Mössbauer spectroscopy. Also, the magnetic properties of the nanoparticles were studied by SQUID magnetometer and optical microscopy. It was suggested that the intermediate iron oxide nanoparticles (before aeration) were formed by the competing processes of oxidation and crystal growth after decomposition of $Fe(CO)_5$. At room temperature, the aerated 5-nm particles were superparamagnetic without interaction among the particles, whereas the 19-nm particles were ferrimagnetic. The 11-nm iron oxide nanoparticles were superparamagnetic with some interactions among the particles.

Introduction

Iron oxide nanoparticles have been of great interest, not only in fundamental properties caused by their multivalent oxidation states, abundant polymorphism, and the mutual polymorphous changes in nanophase, but also in technological applications such as high-density magnetic recording media, sensors, catalysts, and clinical uses.[1−6] Clinical application requires that iron oxide nanoparticles be discrete and superparamagnetic with sizes smaller than 20 nm, and have narrow size distribution for uniform physical and chemical properties.[3,6] Magnetite and maghemite nanoparticles are commonly studied magnetic iron oxides for clinical applications. The advantage of using iron oxide nanoparticles relies on their chemical stability in contrast to that of commonly used nanoparticles of pure Fe metal.

Iron oxide nanoparticles prepared by classical methods[7] have been quite limited to meet the requirement for clinical applications. Recently, thermal decomposition of the iron precursor in hot surfactant solution has been developed for the synthesis of high-quality iron oxide nanoparticles satisfying the requirement. For example, direct decomposition of $FeCup_3$ single precursor can lead to monodisperse maghemite nanoparticles.[8] The thermal decomposition of $Fe(CO)_5$ produces iron nanoparticles and the following oxidation by a chemical reagent can lead to monodisperse maghemite nanoparticles.[9] Also, the high-temperature reaction of iron (III) acetylacetonate in phenyl ether in the presence of alcohol and surfactant can be used to make monodisperse magnetite nanoparticles.[10] Then, the oxidation of magnetite to maghemite nanoparticles requires high temperature (250 °C) and oxygen for 2 h.[10]

Meanwhile, most of the recent advances in the synthesis of high-quality nanoparticles have used highly pure organometallic precursor and precisely controlled inert conditions such as purified high-grade reagents and freeze−thaw technique. An easy and economic synthesis would be desirable for clinical and industrial applications. From the known fast oxidations of unprotected iron nanoparticles[11] and of ferrous ion to ferric

* To whom correspondence should be addressed. E-mail: kjwoo@kist.re.kr.

† Korea Institute of Science and Technology.

‡ Kookmin University.

(1) Cornell, R. M.; Schwertmann, U. *The Iron Oxides*; Wiley-VCH: Weinheim, Germany, 2003.

(2) Cullity, B. D. *Introduction to Magnetic Materials*; Addison-Wesley: Reading, MA, 1972.

(3) Häfeli, U.; Schütt, W.; Teller, J.; Zborowski, M. *Scientific and Clinical Applications of Magnetic Carriers*; Plenum Press: New York, 1997.

(4) (a) Jiang, J. Z.; Lin, R.; Lin, W.; Nielsen, K.; Mørup, S.; Dam-Johansen, K.; Clasen, R. *J. Phys. D* **1997**, *30*, 1459. (b) Sun, H. T.; Cantalini, C.; Faccico, M.; Peline, M. *J. Am. Ceram. Soc.* **1996**, *79*, 927. (c) Matijevic, E.; Scheiner, P. *J. Colloid Interface Sci.* **1978**, *63*, 509. (d) Ozaki, M.; Kratohvil, S.; Matijevic, B. *J. Colloid Interface Sci.* **1984**, *102*, 146.

(5) (a) Benz, M.; van der Kraan, A. M.; Prins, R. *J. Appl. Catal. A* **1998**, *172*, 149. (b) Anantharaman, M. R.; Joseph, K. V.; Keer, H. V. *Bull. Mater. Sci.* **1997**, *20*, 975. (c) Kryder, M. H. *MRS Bull.* **1996**, *21*, 17. (d) Onodera, S.; Kondo, H.; Kawana, T. *MRS Bull.* **1996**, *21*, 35. (e) Watanabe, H.; Seto, J. *Bull. Chem. Soc. Jpn.* **1991**, *61*, 2411. (f) Hong, F. B.; Yang, L.; Schwartz, L. H.; Kung H. H. *J. Phys. Chem.* **1984**, *88*, 2525.

(6) (a) Lubbe, A. S.; Bergemann, C.; Brock, F.; McClure, D. G. *J. Magn. Magn. Mater.* **1999**, *194*, 149. (b) Popplewell, J.; Sakhnini, L. *J. Magn. Magn. Mater.* **1995**, *149*, 72. (c) Pouliquen, D.; Perroud, H.; Calza, F.; Jallet, P.; Lejeune, J. *Magn. Reson. Med.* **1992**, *24*, 75. (d) Lisiecki, I.; Billoudet, F.; Pileni, M. P. *J. Phys. Chem.* **1996**, *100*, 4160. (e) Zhang, Y.; Kohler, N.; Zhang, M. *Biomaterials* **2002**, *23*, 1553.

(7) Kang, Y. S.; Risbud, S.; Rabolt, J. F.; Stroeve, P. *Chem. Mater.* **1996**, *8*, 2209. (b) Hong. C.-Y.; Jang, I. J.; Horng, H. E.; Hsu, C. J.; Yao, Y. D.; Yang, H. C. *J. Appl. Phys.* **1997**, *81*, 4275. (c) Sapieszko, R. S.; Matijevic, E. *J. Colloid Interface Sci.* **1980**, *74*, 405.

(8) Rockenberger, J.; Scher, E. C.; Alivisatos, P. A. *J. Am. Chem. Soc.* **1999**, *121*, 11595.

(9) Hyeon, T.; Lee, S. S.; Park, J.; Chung, Y.; Na, H. B. *J. Am. Chem. Soc.* **2001**, *123*, 12798.

(10) Sun, S.; Zeng, H. *J. Am. Chem. Soc.* **2002**, *124*, 8204.

10.1021/cm049552x CCC: $27.50
Published on Web 06/19/2004

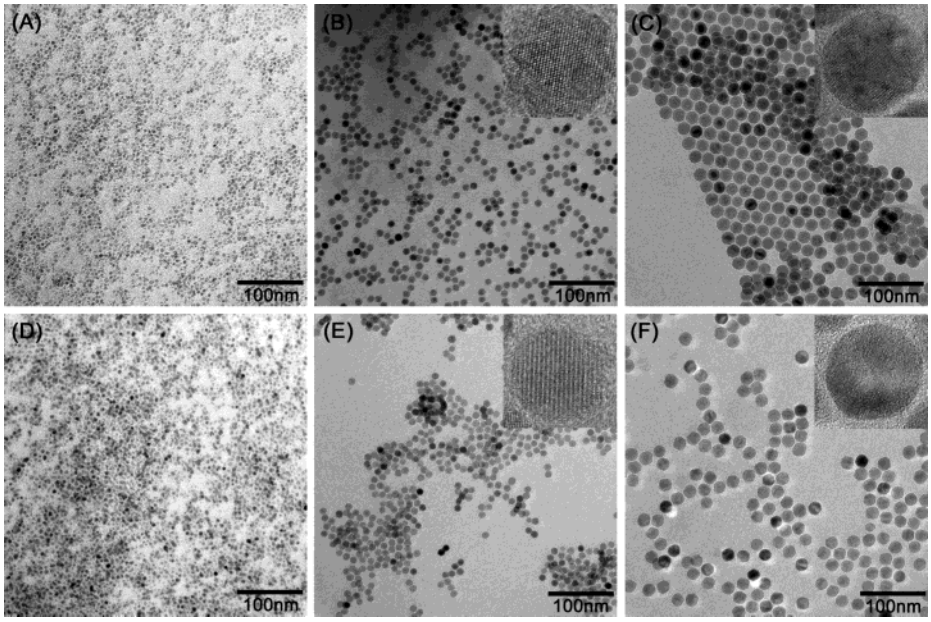

Figure 1. TEM images of respective intermediate and aerated iron oxide nanoparticles: (A) and (D) 5 nm, (B) and (E) 11 nm, (C) and (F) 19 nm; insets are HRTEM images.

ion in the air, we reasoned that iron oxide nanoparticles should be prepared from relatively low-grade reagents and simple aeration.

Here we report an easy synthesis of iron oxide nanoparticles by thermal decomposition of $Fe(CO)_5$ in the presence of the residual oxygen of the system and by consecutive aeration. Compared with the known synthesis[9] of monodisperse maghemite nanoparticles via iron intermediate, we utilized low-grade reagents and solvents as-purchased (without freeze−thaw treatment) and house air, yielding iron oxide nanoparticles as the intermediate. The following further oxidation of iron oxide by aeration and their magnetic properties are investigated.

Experimental Section

According to our easy reaction, 11-nm γ-Fe_2O_3 nanoparticles were synthesized under a nitrogen flow as follows. $Fe(CO)_5$ (0.4 mL, 3.04 mmol, Aldrich, 80−90%) was injected into a mixture containing 20 mL of octyl ether (Aldrich, 99%) and 1.92 mL of oleic acid (6.08 mmol, Aldrich, 90%) at 100 °C. The resulting mixture was slowly heated and refluxed for 2 h. During reflux, the yellow orange mixture changed to colorless and then to dark. This solution was cooled to room temperature (intermediate iron oxide), or aerated for 14 h at 80 °C, and then refluxed for 2 h (aerated iron oxide). The solution was treated with excess ethanol and separated by centrifugation. Similarly, 5- and 19-nm particles were synthesized with varying molar ratios of $Fe(CO)_5$ to oleic acid (1:1 and 1:3 molar ratios, respectively).

For transmission electron microscopy/high-resolution transmission electron microscopy (TEM/HRTEM, Philips CM 200) analysis, a drop of diluted nanoparticle solution in toluene was put onto a carbon-coated copper grid and dried naturally. The X-ray diffraction (XRD, Philips PW 1825) patterns of the particles were recorded using Cu Kα radiation. Mössbauer spectra were recorded at room temperature and 13 or 15 K using a constant-acceleration Mössbauer spectrometer with a ^{57}Co in Rh matrix, and the isomer shift values were reported with respect to the Fe metal. The magnetic data by superconducting quantum interference device (SQUID) were obtained from Korea Basic Science Institute. Optical microscopic images were acquired from camscope.

Results and Discussion

Figure 1 shows the TEM images of intermediate and aerated iron oxide nanoparticles with various sizes. As the molar ratio of oleic acid to $Fe(CO)_5$ increased up to 3, the particle size increased. The higher the molar ratio above 3, the smaller the nanoparticles yielded. This trend agreed with that of the literature report,[9] even though our intermediate was iron oxide nanoparticle (vide infra) whereas the reported intermediate was iron metal nanoparticle. The insets in Figure 1 are the HRTEM images of the corresponding nanoparticles. The TEM/HRTEM images of intermediate iron oxide nanoparticles showed apparent scattering contrast changes within particles. The mixed phase of iron oxides (vide infra) seemed to be one of the major contributing factors to scattering contrast changes.[12] Scattering contrast changes had reduced drastically after aeration. It was considered that the intermediate iron oxides were formed by the competing processes of oxidation and crystal growth after decomposition of $Fe(CO)_5$. The particle size of the nanoparticles showed a trivial change before and after aeration.

Figure 2 represents the XRD patterns of iron oxide nanoparticles before and after the aeration. For the 11-nm particles, the intermediate was composed of wüstite (FeO) and maghemite phases with low crystallinity, whereas the aerated iron oxide was highly crystalline maghemite. The XRD pattern of the aerated 5-nm particles matched with maghemite phase, too. However, the XRD pattern of the 19-nm particles was closer to that of magnetite than maghemite. The larger nanoparticles showed the higher intensity and the narrower peak width as expected. The particle sizes calculated from the XRD data using the Scherrer equation[13] were

(11) Choi, C. J.; Tolochko, O.; Kim, B. K. *Mater. Lett.* **2002**, *56*, 289.

(12) Williams, D. B. *Transmission Electron Microscopy*; Plenum Press: New York and London, 1996.

Table 1. Analyzed Results of Mössbauer Spectra for Iron Oxide Nanoparticles

particle size (nm)	temp (K)	fitted spectrum	hyperfine field (T)	quadruple splitting (mm/s)	isomer shift (mm/s)	line width (mm/s)	area (%)	Fe ion state
5[a]	300	doublet		0.71	0.20	0.93	100	+3
5[a]	13	sextet	51.7	0.00	0.35	0.56	40.3	+3
		sextet	49.0	0.02	0.31	0.90	59.7	+3
11[b]	300	sextet	40.4	0.04	0.34	2.17	75.2	+3
		singlet		0.02	0.93	0.61	21.5	+2
		doublet		0.70	0.05	0.37	3.3	
11[b]	15	sextet	51.0	0.04	0.36	0.82	74.6	+3
		sextet	39.1	0.16	1.04	1.62	22.0	+2
		doublet		0.38	0.13	0.73	3.4	
11[a]	300	sextet	41.8	0.02	0.23	1.73	87.6	+3
		doublet		1.54	0.26	1.53	12.4	+3
11[a]	13	sextet	52.8	0.02	0.35	0.59	73.6	+3
		sextet	50.9	0.02	0.26	0.60	26.4	+3
19[a]	300	sextet	47.0	0.02	0.14	0.58	47.6	+3
		sextet	44.7	0.03	0.56	0.58	52.4	+2.5
19[a]	13	sextet	51.8	0.01	0.33	0.67	84.1	+3
		sextet	48.2	0.03	0.83	0.70	15.9	+2

[a] Aerated particles. [b] Intermediate particles.

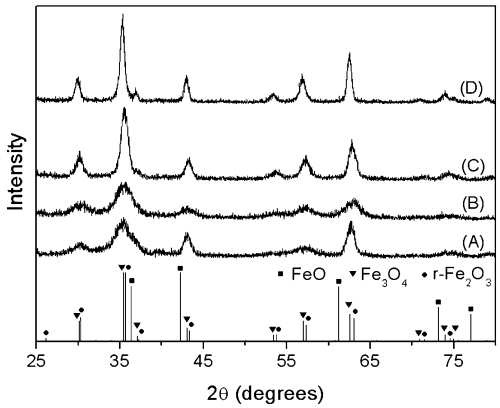

Figure 2. XRD patterns of iron oxide nanoparticles: (A) intermediate 11-nm, and aerated (B) 5-nm, (C) 11-nm, and (D) 19-nm particles. The standard XRD patterns for FeO, Fe_3O_4, and γ-Fe_2O_3 were drawn from the respective JCPDS files 46-1312, 19-629, and 39-1346.

5.2, 11.1, and 18.9 nm and matched well with those (5, 11, and 19 nm; average over 100 particles) obtained from the TEM images. The repeated aeration and heating (168 °C) of magnetite evolved maghemite nanoparticles. However, the repeated aeration and reflux could not convert maghemite to hematite (α-Fe_2O_3), which is the most stable phase of iron oxides thermodynamically.[1,14] The aeration alone, without reflux, of the intermediate solution transformed to maghemite with a trivial change in XRD peak intensity.

Because magnetite and maghemite have very similar XRD patterns, we performed further characterization by Mössbauer spectroscopy to distinguish the phases of iron oxide nanoparticles. Figure 3 A and B show the Mössbauer spectra of 11-nm particles before and after the aeration. The original data of intermediate nanoparticles were fitted into a singlet, a doublet, and a sextet at 300 K and into a doublet and two sextets at 15 K. Those of aerated nanoparticles were fitted into a doublet and a sextet at 300 K and into two sextets at 13 K. The analyzed results are summarized in Table 1. For the intermediate iron oxides, a singlet at 300 K has been converted into a sextet at 15 K with the isomer shift changes from 0.93 to 1.04 mm/s relative to the Fe metal. The isomer shift values matched well with the reported value (0.95 mm/s)[1,15] of wüstite phase. The singlet to sextet conversion suggested a magnetic property change of wüstite nanoparticles from paramagnetic at 300 K to ferrimagnetic at 15 K. In case of a sextet, the isomer shift values smaller than 0.5 mm/s suggested Fe^{3+} ion state.[15] Referring to this analysis and the XRD data, the sextet constituting about 75% of the intermediate at each temperature was considered as the maghemite nanoparticles. The phase of a doublet was not certain. Therefore, the intermediate nanoparticles were considered as a mixture of wüstite, maghemite, and 3% of unknown phase. For the aerated iron oxide, the isomer shift values suggested[15] that the valence state is Fe^{3+}. So, the aerated phase was thought to be maghemite with partial superparamagnetic property at 300 K and with ferrimagnetic property at 13 K. The narrowing of the spectral lines and increase of the hyperfine magnetic field of 13 K spectrum after aeration seemed to be caused by increased crystallinity.

The Mössbauer spectra of the aerated 5- nm particles showed a remarkable contrast to those of the aerated 19-nm particles (Figure 3C vs D). The spectrum of 5-nm particles displayed a doublet pattern at 300 K, representing a superparamagnetic property. The spectrum at 13 K was fitted into two sextet patterns, showing ferrimagnetic property. The phase of 5-nm particles was considered as maghemite from the isomer shift values (0.20 mm/s at 300 K, and 0.35 and 0.31 mm/s at 13 K) relative to the Fe metal and the XRD data. The spectrum of 19-nm particles at 300 K was fitted into two sextet patterns. The two sextets were compared with a typical Mössbauer spectrum[1] of magnetite. Typically, the room-temperature spectrum of magnetite consists of two sextets, one corresponding to high spin Fe^{3+} on the tetrahedral sites (hyperfine field = 49.2 T) and the other corresponding to $Fe^{2.5+}$ on the octahedral sites.[1] Electron dislocation caused the nucleus to sense

(13) Jenkins, R.; Snyder, R. L. *Introduction to X-ray Powder Diffractometry*; Wiley-Interscience: New York, 1996.

(14) (a) Zboril, R.; Mashlan, M.; Petridis, D. *Chem. Mater.* **2002**, *14*, 969. (b) Xu, X. N.; Wolfus, Y.; Shaulov, A.; Yeshurun, Y.; Felner, I.; Nowik, I.; Koltypin, Yu.; Gedanken, A. *J. Appl. Phys.* **2002**, *91*, 4611.

(15) Shenoy, G. K.; Wagner, F. E. *Mössbauer Isomer Shifts*; North-Holland: Amsterdam, 1978.

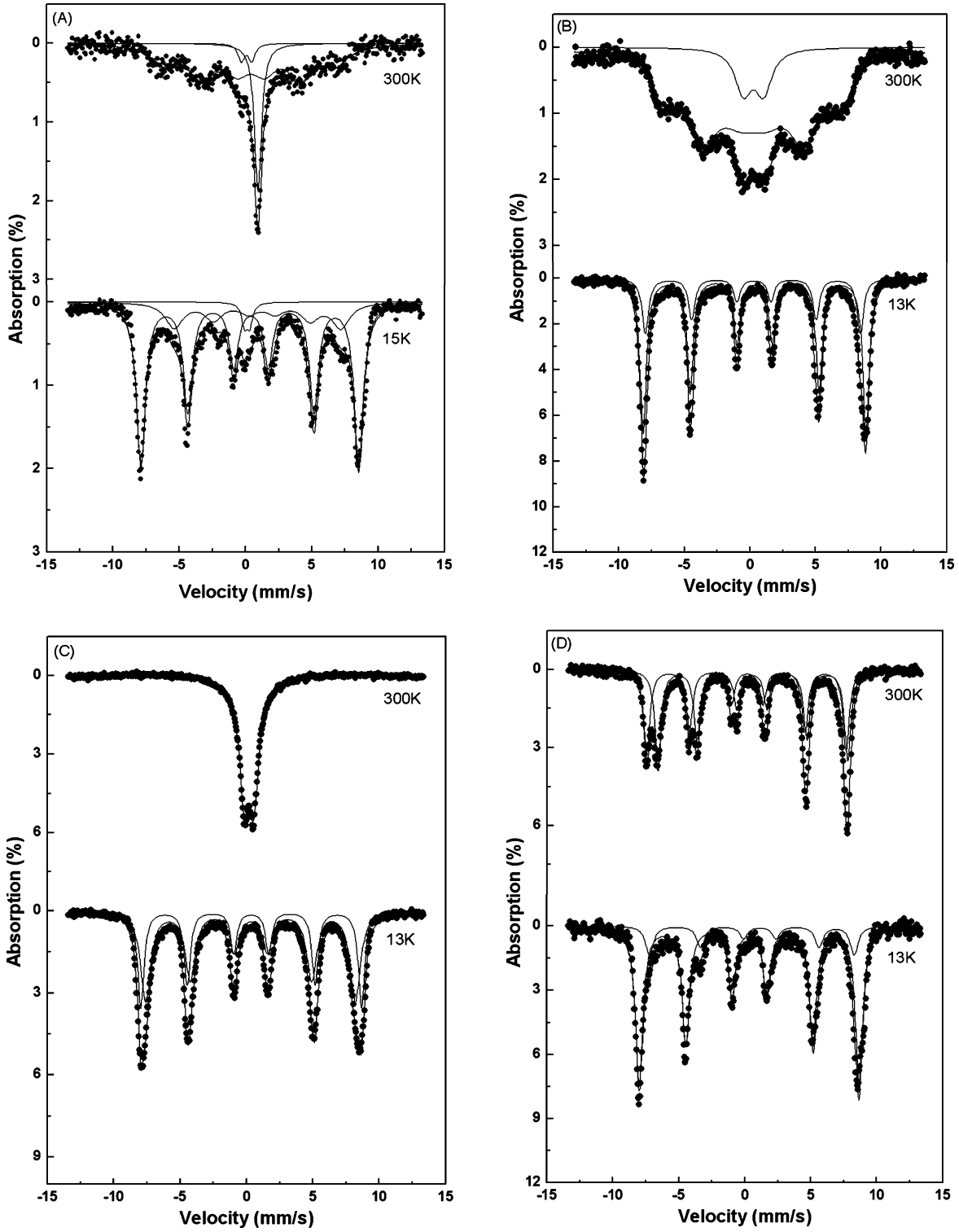

Figure 3. Mössbauer spectra of iron oxide nanoparticles: (A) intermediate 11 nm, and aerated (B) 11 nm, (C) 5 nm, (D) 19 nm.

one average valence (hyperfine field = 46.1 T). It is known that small particle sizes reduce the hyperfine field below that of the bulk material and broaden the resonance lines.[1] The two sextets with quadruple splitting, hyperfine field, and isomer shift of one (0.02 mm/s, 47.0 T, and 0.14 mm/s) and the other (0.03 mm/s, 44.7 T, and 0.56 mm/s) relative to the Fe metal, suggesting the existence of Fe^{3+} and $Fe^{2.5+}$ ionic states,[15] was considered as ferrimagnetic magnetite. The ratio of the spectrum areas corresponding to the tetrahedral A (47.6) and octahedral B (52.4) sites in the magnetite structure deviated from an ideal value of A/B = $^1/_2$, possibly implicating further oxidation and incomplete crystallization during the aeration process. Fitting of the 13 K spectrum is expected to be more complex than two sextets due to Verwey transition.[16] Going into further detail regarding the sub-spectrum is beyond the scope of this report. Comparison with a typical magnetite spectrum[16] at low temperature below Verwey transition supported magnetite phase of 19-nm particles. It

(16) Van Diepen, A. H. *Physica* **1977**, *86−88 B*, 955.

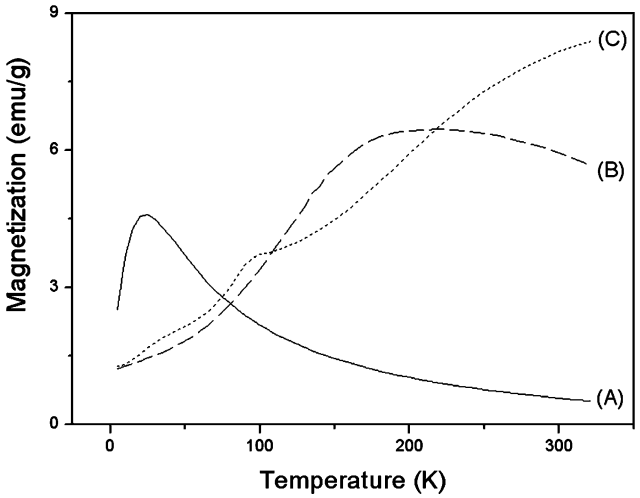

Figure 4. Zero field cooling curves of aerated nanoparticles under an applied field of 100 Oe: (A) 5-nm particles, (B) 11-nm particles, and (C) 19-nm particles.

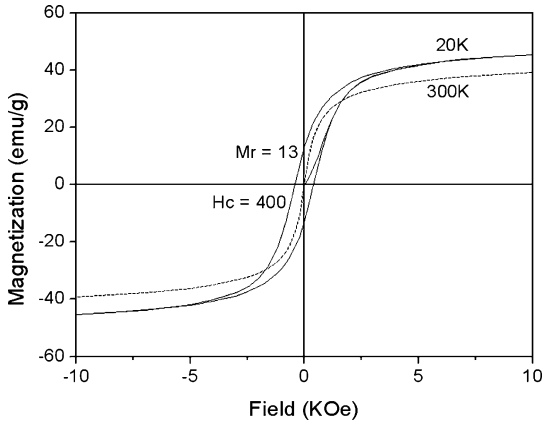

Figure 5. Hysteresis curves of 11-nm aerated particles.

is not certain yet why the smaller nanoparticles (5 and 11 nm) prefer maghemite phase while the larger nanoparticles (19 nm) prefer magnetite phase. Further study is under way to investigate a relationship between particle size and phase.

Figure 4 shows the zero field cooling curves of aerated nanoparticles recorded by a SQUID magnetometer. The zero field cooling curves of 5- and 11-nm particles show the blocking temperatures at around 30 and 215 K, respectively. The curve (A) decreases rapidly with temperature and suggests[17] that 5-nm particles are superparamagnetic with little interaction among the particles. The curve (B) decreases slowly with temperature and indicates[17] that 11 nm particles are superparamagnetic, with some interactions among the particles. The magnetization curve for 19-nm particles shows a constantly increasing trend with the temperature up to 323 K, representing a ferrimagnetic property at room temperature.

Figure 5 shows the hysteresis curves of the aerated 11-nm particles. The coercivity and remanence values

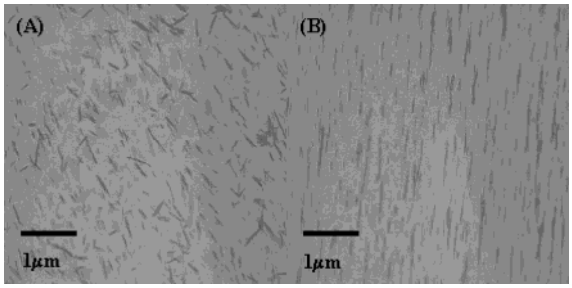

Figure 6. Optical microscopic images of 11-nm intermediate particles: (A) without and (B) with an external magnetic field.

are not discernible at 300 K, indicating a superparamagnetic behavior, and 400 Oe and 13 emu/g, respectively, at 20 K, showing a ferrimagnetic behavior. Neither the hysteresis curves of the 5- or 19-nm particles (Supporting Information) showed discernible coercivity and remanence at 300 K. The magnetization at 2 T and 300 K was 23, 42, and 46 emu/g for the respective 5-, 11-, and 19-nm particles. The smaller magnetizations than their respective bulk values (73.5 emu/g for maghemite and 92 emu/g for magnetite) are likely due to the mass of the surfactant, the existence of a surface layer with reduced magnetization, and some diamagnetic contribution from the surfactant shell.[18]

Figure 6 shows the optical microscopic images of 11-nm particles by an external magnetic field. The sample was prepared by placing a drop of toluene-diluted solution of nanoparticles on a glass plate and an external field was applied before the evaporation of the solvent. The nanoparticles in diluted solution were randomly self-assembled in a 2-dimensional way without external field, but were aligned in a parallel way with an applied magnetic field. It was certain that 11-nm iron oxide nanoparticles were aligned along the field direction and superparamagnetic with some interactions among the particles.

We have described the easy preparation of iron oxide nanoparticles (5- and 11-nm maghemite and 19-nm magnetite) by thermal decomposition of $Fe(CO)_5$ in the presence of residual oxygen of the system and by consecutive aeration. The 11-nm iron oxide nanoparticles at any phase from the intermediate to the aerated were partially superparamagnetic with some interactions among the particles. The 5-nm particles were superparamagnetic without interaction among the particles, whereas the 19-nm particles were ferrimagnetic.

Acknowledgment. This research has been conducted under the future key technology program sponsored by the Minister of Science and Technology in Korea.

Supporting Information Available: Hysteresis curves (PDF) of 5- and 19-nm particles. This material is available free of charge via the Internet at http://pubs.acs.org.

CM049552X

(17) Bødker, F.; Hansen, M. F.; Koch, C. B.; Lefmann, K.; Mørup, S. *Phys. Rev. B*, **2000**, *61*, 6826.

(18) Saravanan, P.; Alam, S.; Mathur, G. N. *J. Mater. Sci. Lett.* **2003**, *22*, 1283.